

SPECTROSCOPY OF THE TYPE IC SUPERNOVA SN 2017IUK ASSOCIATED WITH LOW-REDSHIFT GRB 171205A

J. WANG,^{1,2} Z. P. ZHU,^{3,1} D. XU,¹ L. P. XIN,¹ J. S. DENG,^{1,2} Y. L. QIU,¹ P. QIU,⁴ H. J. WANG,⁴ J. B. ZHANG,⁴ AND
J. Y. WEI^{1,2}

¹*Key Laboratory of Space Astronomy and Technology, National Astronomical Observatories, Chinese Academy of Sciences, Beijing 100101, China*

²*School of Astronomy and Space Science, University of Chinese Academy of Sciences, Beijing, China*

³*School of Physics, Huazhong University of Science and Technology, Wuhan 430074, China*

⁴*Key Laboratory of Optical Astronomy, National Astronomical Observatories, Chinese Academy of Sciences, Beijing 100101, China*

(Received July 1, 2016; Revised September 27, 2016; Accepted March 10, 2024)

Submitted to ApJ

ABSTRACT

We here report a spectroscopic monitor for the supernova SN 2017iuk associated with the long-duration low-luminosity gamma-ray burst GRB 171205A at a redshift of 0.037, which is up to now the third GRB-SN event away from us. Our spectroscopic observations and spectral analysis allow us to identify SN 2017iuk as a typical broad-line type Ic SN. A comparison study suggests that the type-IcBL SN 2017iuk resembles to SN 2006aj in following aspects: 1) similar spectra at the nearby epochs, 2) comparable evolution of the photospheric velocity obtained from the measurements based on both Si II λ 6355 line and spectral modeling, and 3) comparable explosion parameters. This analogy could imply a formation of a neutron star in the core-collapse of GRB 171205A/SN 2017iuk as previously suggested in GRB 060218/SN 2006aj. The properties of the host galaxy is discussed, which suggests that GRB 171205A/SN 2017iuk occurred in an early type (S0), high-mass, starforming galaxy with low specific SFR and solar metallicity.

Keywords: supernovae: individual: SN 2017iuk — gamma-ray burst: individual: GRB 171205A — techniques: spectroscopic — methods: observational

Corresponding author: J. Wang
wj@bao.ac.cn

Corresponding author: Z. P. Zhu
zipei@hust.edu.cn

Corresponding author: D. Xu
dxu@nao.cas.cn

1. INTRODUCTION

The connection between long-duration gamma-ray bursts (LGRBs) and their associated broad-line type Ic supernovae (SNe IcBL) with an absolute magnitude of $M_V \sim -19$ mag has been firmly established in past two decades due to the prompt spectroscopic follow-up observations (see reviews in Woosley & Bloom 2006; Hjorth & Bloom 2012; Cano et al. 2017 and references therein). So far, the GRB-SN association has been identified in about 30 events with a redshift range from 0.00867 (GRB 980425/SN1998bw, e.g., Galama et al. 1998) to 1.0585 (GRB 000911, e.g., Lazzati et al. 2001; Masetti et al. 2005), although a non-association was firmly identified in two low- z cases: GRB 060505 and GRB 060614 by deep imaging (Fynbo et al. 2006; Della Valle et al. 2006; Gal-Yam et al. 2006).

Study of the SNe associated with LGRBs is important for exploring the nature of death of massive stars. Even though it is widely accepted that LGRBs originate from core-collapse of young massive stars (e.g., Woosley & Bloom 2006; Hjorth & Bloom 2012; Wang et al. 2018 and references therein), the compact objects formed in the core-collapse are still under hot debate. They could be either a stellar-mass blackhole (e.g., Woosley 1993; MacFadyen & Woosley 1999) or a magnetar (i.e. a rapidly rotating neutron star with extremely large magnetic field, e.g., Dai & Lu 1998; Woosley & Heger 2006; Zhang & Dai 2010; Bucciantini et al. 2007; Mazzali et al. 2014; Wang et al. 2017). In fact, the SN explosion mechanism depends on the compact objects formed in the core-collapse. For instance, two types of central engines, i.e., 1) radioactive-heating caused by the radioactive decay of nickel and cobalt, and 2) rotation energy of a magnetar, have been proposed for the powering of the SNe associated with LGRBs (e.g., Greiner et al. 2015; Cano et al. 2016, 2017; Metzger et al. 2015; Bersten et al. 2016; Sukhbold et al. 2016; Wang et al. 2015; Dai et al. 2016; Iwamoto et al. 2000; Nakamura et al. 2001; Maeda et al. 2003).

Among the identified LGRB-SN events, only two cases, i.e., GRB 980425/SN1998bw and GRB 060218/SN2006aj (e.g., Pian et al. 2006; Mazzali et al. 2006) are found to be at redshift less than 0.05 (~ 200 Mpc). Both them can be classified as low-luminosity GRBs (*ll*GRBs) with an isotropic γ -ray luminosity of $\log L_{\gamma, \text{iso}} < 48.5$. In this paper, we report a spectroscopic study for the type-IcBL SN 2017iuk associated with GRB 171205A at a redshift of 0.037, which is up to now the third GRB-SN event away from us.

The paper is organized as follows. Section 2 summarizes the basic properties of GRB 171205A/SN2017iuk. The spectroscopic observations and data reductions of

SN 2017iuk are presented in Section 3. Section 4 shows the analysis and results, A conclusion and implications are presented in Section 5. A Λ CDM cosmology with parameters $H_0 = 70 \text{ km s}^{-1} \text{ Mpc}^{-1}$, $\Omega_m = 0.3$, and $\Omega_\Lambda = 0.7$ is adopted throughout the paper.

2. GRB 171205A AND ASSOCIATED SN 2017IUK

GRB 171205A was detected by *Swift* Burst Alert Telescope (BAT) on December 05, 2017 at 07:20:43 UT (*Swift* trigger 794972, D’Elia et al. 2017a). *Swift* XRT detected a bright new X-ray source at 144.7 seconds after the BAT trigger (D’Elia et al. 2017b). The BAT on-ground analysis (Barthelmy et al. 2017) reported a duration of $T_{90} = 189.4 \pm 35.0$ s, a fluence of $(3.6 \pm 0.3) \times 10^{-6} \text{ erg cm}^{-2}$ in the 15-150 keV band, and a powerlaw spectrum with a photon index of $\Gamma = 1.41 \pm 0.14$. A photon index of $\Gamma = 1.717^{+0.035}_{-0.024}$ within the 0.3-10 keV band was reported by a refined XRT analysis (Kennea et al. 2017). The burst was also detected by Konus-Wind with a well fitted a powerlaw spectrum with a $\Gamma = 2.0 \pm 0.14$ in the 20-1500 keV band (Frederiks et al. 2017). The reported fluence of $(7.8 \pm 1.6) \times 10^{-6} \text{ erg cm}^{-2}$ corresponds to an isotropic energy of $E_{\text{iso}} \sim 6.6 \times 10^{49} \text{ erg}$ in the 1-10000keV band, and to a $\log L_{\gamma, \text{iso}} = 47.5$, which allows us to classify GRB 171205A as a *ll*GRB.

The afterglow of GRB 171205A was observed in multi-wavelength from near-ultraviolet to radio (e.g., Izzo et al. 2017; Butler et al. 2017; Mao et al. 2017a,b; de Ugarte Postigo et al. 2017a; Choi et al. 2017; Melandri et al. 2017; Ramsay et al. 2017; Cobb et al. 2017; Smith & Tanvir 2017; Laskar et al. 2017; Perley et al. 2017). The spectroscopic observation performed by VLT at 1.5hr after the trigger detected an optical transient at the position R.A.(J2000) = $11^{\text{h}}09^{\text{m}}39.573\text{s}$ and Dec(J2000) = $-12^{\circ}35'17.37''$, which is at the outskirts of the galaxy 2MASX J11093966-1235116 with a redshift of 0.037. The spectrum shows evident $\text{H}\alpha$, $[\text{N II}]\lambda 6583$ and $[\text{S II}]\lambda\lambda 6716, 6731$ emission lines at the same redshift of the galaxy. The detection of an associated SN (SN 2017iuk) was reported in December 07, 2017 by a follow-up spectroscopic observation using the 10.4m GTC telescope (de Ugarte Postigo et al. 2017b). The SN spectrum at that epoch is reported to be similar to the very early spectra of SN1998bw, which is further confirmed in Prentice et al. (2017).

3. OBSERVATIONS AND DATA REDUCTIONS

Our spectroscopic observations and data reductions are described in this section.

3.1. Observations

The long-slit spectra of GRB 171205A/SN 2017iuk were obtained by the NAOC 2.16m telescope at Xing-long observatory (Fan et al. 2016) at five epochs, i.e., December 17, 21, 25, 28 and 30. Figure 1 shows the R-band image of the field of GRB 171205A taken by the 2.16m telescope at December 28, 2017. Our spectroscopic observations were carried out with the Beijing Faint Object Spectrograph and Camera (BFOSC) equipped with a back-illuminated E2V55-30 AIMO CCD as the detector. The grating G4 and a slit of width of $1.8''$ oriented in the south-north direction were used in all the five observation runs. This setup finally results in a spectral resolution of $\sim 10\text{\AA}$ as measured from the sky emission lines and comparison arcs, and provides a wavelength coverage from 3850\AA to 8000\AA . Except for the observation run at December 21, 2017, the target was observed twice in succession in each run. The exposure time of each frame ranges from 1800 to 4800s, depending on both brightness of the object and weather condition. In each run, the wavelength calibration and flux calibration were carried out by the iron-argon comparison arcs and by the Kitt Peak National Observatory (KPNO) standard stars (Massey et al. 1988), respectively. The spectra of the standard stars were observed with the same instrumental setups immediately after the exposure of the object.

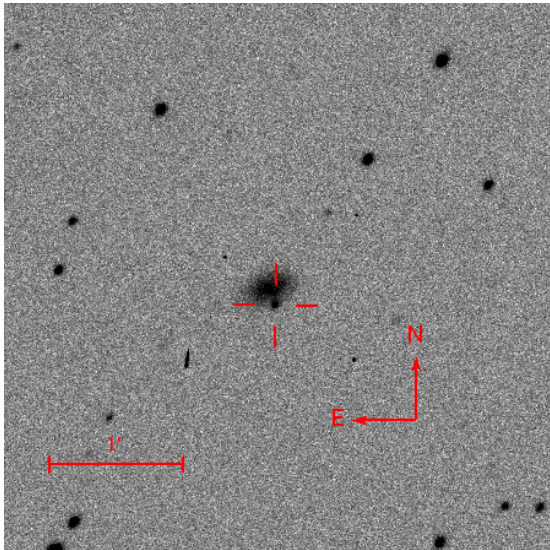


Figure 1. R-band image of GRB 171205A/SN 2017iuk and its host galaxy 2MASX J11093966-1235116, which was taken at December 28, 2017, i.e., +23d after the trigger of the GRB. North is up, and east the left. The angular scale of the image is shown at the left-bottom corner. The burst, marked by the red cross, occurs at the outskirts of the host.

3.2. Data reductions

Standard procedures were adopted to reduce the two-dimensional spectra by using the IRAF package¹. The data reduction includes bias subtraction, flat-field correction, and image combination along with cosmic-ray removal before the extraction of the one-dimensional spectra². The contamination due to the underlying host galaxy was taken into account in our extraction through background subtraction. In order to reproduce the gradient of the surface brightness profile of the host, the level of the underlying background is determined by a linear fitting in the two selected background regions. All the extracted one-dimensional spectra were then calibrated in wavelength and flux by the corresponding comparison arc and standards. The flux calibration was performed by comparing the observed spectra of the standards with the spectrophotometrically calibrated spectra provided in the IRAF package, which corrects the specific response of both telescope and spectrograph and the extinction due to Earth's atmosphere. The A-band telluric feature around $\lambda\lambda 7600\text{--}7630$ due to O_2 molecules was removed from each observed spectrum by the corresponding standard. The Galactic extinction was corrected by the extinction magnitude of $A_V = 0.138$ (Schlafly & Finkbeiner 2011) taken from the NASA/IAPC Extragalactic Database (NED), assuming the $R_V = 3.1$ extinction law of our Galaxy (Cardelli et al. 1989). The spectra were then transformed to the rest frame, along with the correction of the relativity effect on the flux, according to the redshift of 0.037 of the host galaxy.

4. ANALYSIS AND RESULTS

4.1. Identification and evolution

Figure 2 shows the spectral evolution of SN 2017iuk in the period from +12 to +30day. The first spectrum taken at +12 days after the onset of the GRB is very blue and featureless, except for the notch at $\sim 6000\text{\AA}$ caused by the Si II $\lambda 6355$ absorption feature and the two peaks around 4500\AA and 5300\AA . The latter two features are resulted from the Fe II $\lambda 5169$ absorption (e.g., Filippenko 1997). All these features are quite typical for other GRB-SN events (e.g., Cano et al. 2017; D'Elia et al. 2015), which allows us to classify SN 2017iuk as a SN IcBL with a highly stripped progenitor.

¹ IRAF is distributed by the National Optical Astronomical Observatories, which is operated by the Association of Universities for Research in Astronomy, Inc., under cooperative agreement with the National Science Foundation.

² The image combination is skipped for the spectrum taken at December 21, 2017 since there was only one exposure. The cosmicray removal was performed on the single exposure before spectral extraction.

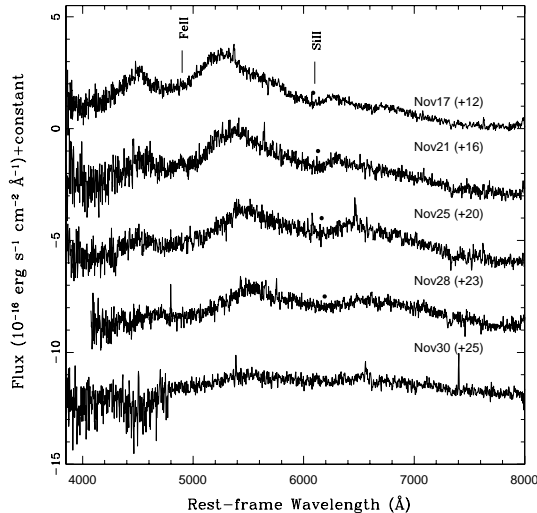


Figure 2. Spectroscopic time-series of type IcBL SN 2017iuk at the five different epochs from December 17 to 30, 2017. All the spectra are transformed to the rest frame based on the redshift of 0.037, and are shifted vertically by an arbitrary amount for visibility. The Fe II $\lambda 5169$ and Si II $\lambda 6355$ absorption features are marked on the first spectrum. The black dots show the evolution of the position of the Si II $\lambda 6355$ absorption.

One can see from Figure 2 that the two peaks at $\sim 4500\text{\AA}$ and $\sim 5300\text{\AA}$ gradually weaken from +12 to 23day, along with a gradual redshift for the $\sim 5300\text{\AA}$ feature. The bottom spectrum shows that the emission from SN 2017iuk fades out at +30day, in which there are marginal $\sim 5300\text{\AA}$ feature and extremely weak [O I] $\lambda\lambda 6300, 6363$ broad emission that is commonly detected in the nebular phase (e.g., Filippenko 1997).

Figure 3 compares the spectrum of SN 2017iuk taken at December 17, 2017 (+12day), which is close to the R-band light peak (Wang, X. G. et al. private communication), to the spectra of SN 1998bw and SN 2006aj at the similar epochs. Our comparison clearly suggests an analogy between SN 2017iuk and SN 2006aj.

4.2. Photospheric velocity

The photospheric expansion velocity in Type Ibc SNe is traditionally estimated from the Fe II lines at $\sim 5000\text{\AA}$, because compared to the Fe II lines the other ones are produced far above the photosphere. However, this method is unavailable for SNe IcBL due to their high velocities that result in a line identification difficulty because of the heavy line blending.

We here attempt to estimate photospheric velocity of SN 2017iuk by using the absorption trough of the Si II $\lambda 6355$ line (e.g., Sahu et al. 2018), except for the last spectrum taken at December 30, 2017. In the last spec-

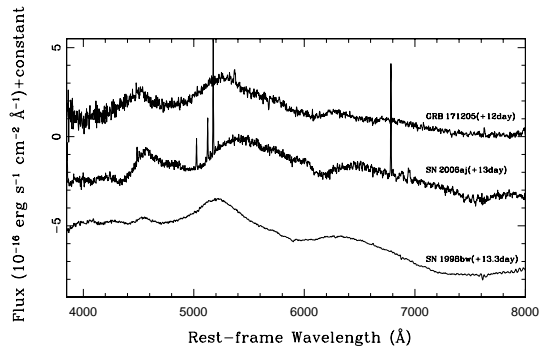


Figure 3. A comparison of the spectrum of SN 2017iuk taken at December 17, 2017 (+12day) to those of SN 1998bw (+13.3day) and SN 2006aj (+13.0day) at the similar epochs.

trum, the Si II $\lambda 6355$ feature is too weak to be measured. We mark the positions of the Si II $\lambda 6355$ line by dots in Figure 2, which clearly shows an evolution of the expansion of photosphere with a gradually decreasing velocity. The Si II-based photospheric velocities (see Column (2) in Table 1) decrease from 12,000 to 8,000 km s^{-1} in the period from +12 to +23day. This temporal evolution of photospheric velocity is compared to the photospheric velocities of other type Ic SNe measured from the Si II line in Figure 4. One can again identify an analogy to SN 2006aj from the evolution of photospheric velocity.

Table 1. Photospheric velocities and blackbody temperatures measured from the spectra

Date	$v_{\text{ph}}(\text{SiII})$ km s^{-1}	$v_{\text{ph}}(\text{syn})$ km s^{-1}	T_{bb} K
(1)	(2)	(3)	(4)
Dec 17, 2017	12700 ± 1100	12000 ± 1000	12000
Dec 21, 2017	10600 ± 1000	10000 ± 1000	8000
Dec 25, 2017	10300 ± 1800	10000 ± 2000	6000
Dec 28, 2017	7800 ± 2000

4.3. Spectral modeling with SYN++

In this section, we model the spectra of the SN 2017iuk through the synthetic spectra generated by the SYN++ code (Thomas et al. 2011) that is an enhanced version of the parameterized supernova spectrum synthesis code SYNOW (Fisher 2000; Branch et al. 2000). In generat-

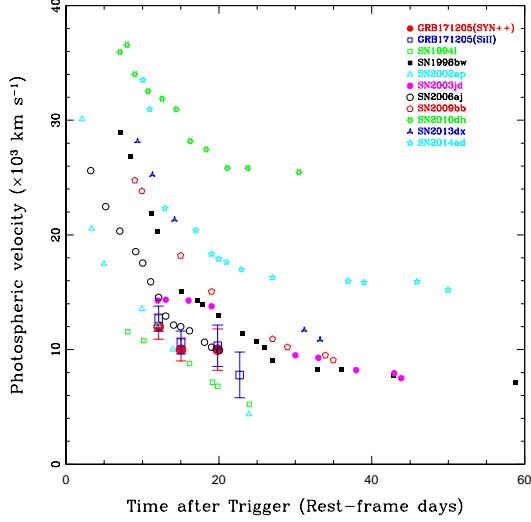


Figure 4. Temporal evolution of the photospheric velocity of SN 2017iuk. The blue open squares mark the photospheric velocities measured from the Si II $\lambda 6355$ absorption feature, and the red solid circles the velocities obtained from the fitting based on the synthetic spectra generated by SYN++. The temporal evolutions of photospheric velocities of other type Ic SNe measured from the Si II $\lambda 6355$ features are plotted for a comparison. The data are taken from Sahu et al. (2018).

ing synthetic spectra, the exciting temperature is fixed to be 6,000K, and the involved ions include Fe II, Co II, Si II, Ca II, Mg II and O I. Based on the synthetic spectra, we fit the observed rest-frame spectra over the whole spectroscopic wavelength range through “chi-by-eye” by changing the blackbody temperature, the optical depth of each ion, and the velocity of the photosphere. The fittings are schemed in Figure 5 for the spectra taken at December 17, 21 and 25, 2017. One can see from the figure that in all the three cases the generated synthetic spectra generally match the observed ones quite well, except for the “blue wing” of the $\sim 5000\text{\AA}$ feature. This failure of reproducing might be due to the imperfect of the adopted atomic data of iron, especially when the photospheric temperature is low. The best-fitted photospheric velocities decrease from 12,000 to 10,000 km s^{-1} within the period from +12 to +20d after the trigger of the GRB. The best-fitted velocities are overplotted in Figure 4, which shows a significant consistence with the measurements based on the Si II absorption. In the period, the modeled blackbody temperatures decrease from 12,000 to 6000K. The modeled photospheric velocities and blackbody temperatures are tabulated in Table 1 (columns (3) and (4)).

5. CONCLUSION AND DISCUSSION

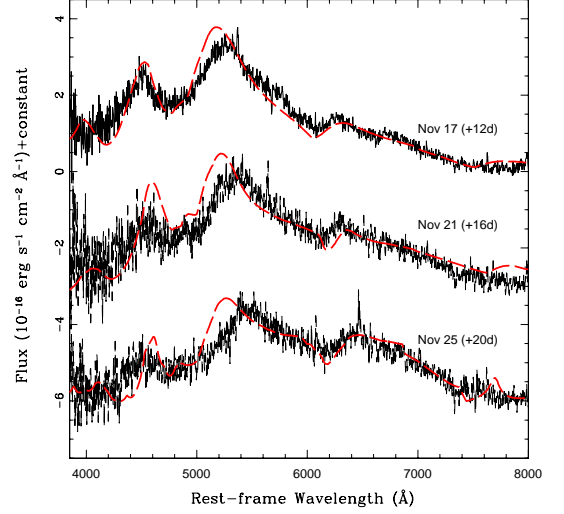


Figure 5. An illustration of the spectral fitting based on the synthetic spectra generated by using SYN++.

We monitored SN 2017iuk associated with the *ll*GRB GRB 171205A in spectroscopy, which is up to now the third GRB-SN event away from us. Our spectroscopy observations and spectral analysis enable us to identify the SN as a broad-line type Ic SN. A comparison study suggests that SN 2017iuk resembles to SN 2006aj due to their 1) similar spectra at the similar epochs and 2) consistent evolutions of photospheric velocity.

5.1. Explosion parameters and mechanism

In this section, we estimate the explosion parameters from our spectral analysis presented in Section 4, and argue that the estimated parameters roughly agree with those of SN 2006aj, which reinforces the analogy revealed in the above section.

We estimate the mass of ejecta M_{ej} from the evolution of photospheric velocity by assuming an exponential density profile $\rho = \rho_0 e^{-v/v_e}$, where ρ_0 is the central density and v_e the e-folding velocity. The evolution of photospheric velocity can be therefore expressed as (Eq. 3 in Deng et al. 2001)

$$v_{\text{ph}} \approx -v_e \ln \left[10^{-6} \frac{\tau_{\text{ph}}}{\bar{\kappa}} \left(\frac{v_e}{10^3 \text{ km s}^{-1}} \right)^2 \left(\frac{M_{\text{ej}}}{M_{\odot}} \right)^{-1} \right] - 2v_e \ln t_d \quad (1)$$

where τ_{ph} is the optical depth at the photosphere, $\bar{\kappa}$ the optical opacity and t_d the time since explosion in unit of day. With the measured v_{ph} , we fitted the evolution of v_{ph} as $v_{\text{ph}} = a + b \ln t_d$. After deriving a value of v_e from the best fitted b ($= -2v_e$), the ejecta mass is inferred to be $M_{\text{ej}} \approx 1.1 M_{\odot}$ from the best fitted value of a , where the typical values of $\tau_{\text{ph}} = 1$ and $\bar{\kappa} = 0.07 \text{ cm}^2 \text{ g}^{-1}$ are adopted in the estimation. The explosion kinetic energy

is then estimated to $E_k = 6M_{\text{ej}}v_e^2 = 1.4 \times 10^{51}$ erg by integrations of both ρ and ρv^2 over velocity. Although the inferred M_{ej} and E_k are within the ranges of the typical values of SNe IcBL, they are at the lower end of the distributions of the GRB-associated SNe IcBL that have the typical values of $M_{\text{ej}} \sim 1 - 10M_\odot$ and $E_k \sim 1 \times 10^{52}$ erg (e.g., Cano et al. 2017).

We alternatively estimate E_k by using the expression of $E_k = 3/10 M_{\text{ej}} v_{\text{ph}}^2$ given in Arnett (1982, 1996). The photospheric velocity at the time of bolometric maximum, i.e., +12d after the trigger, results in a value of $E_k \approx 9 \times 10^{50}$ erg, which is roughly consistent with the above value that is estimated from v_e . The E_k/M_{ej} ratio is resulted to be ~ 0.13 for SN 2017iuk.

We argue that the explosion parameters estimated above are comparable to those of SN 2006aj (see Table 3 in Cano et al. 2017). The comparable explosion parameters and the revealed similarity in the spectral evolution motivate us to suspect that SN 2017iuk/GRB 171205A is of the similar explosion mechanism to SN 2006aj/GRB 060218. By a detailed modeling of the light curve and spectra, Mazzali et al. (2006) suggested that SN 2006aj/GRB 060218 is produced by a core-collapsing of a massive star with an initial mass of $\sim 20M_\odot$, which expects a formation of a neutron star rather than a black hole after the core-collapse.

5.2. Host galaxy

The host galaxy 2MASX J11093966-1235116 (LCRS B110709.2-121854) of GRB 171205A/SN 2017iuk is classified as a S0 galaxy in the Lyon Extragalactic Database (LEDa). The poor seeing ($2.5-3''$) of our observations, however, prevent us from further morphological study on the galaxy. We estimate the total stellar mass (M_\star) of the galaxy from its K-band photometry, because the near-infrared emission traces the mass of late-type stars better and is much less sensitive to extinction by dust. With the distance modulus of $\mu = 35.90 \pm 0.15\text{mag}$, the absolute magnitude in K_s -band is obtained to be $-23.57 \pm 0.21\text{mag}$, which yields a luminosity in K_s -band of $L_K = 5.5 \times 10^{10} L_\odot$ by adopting an absolute solar K_s band magnitude of 3.29 (Blanton & Roweis 2007). Adopting a universal K_s -band mass-to-light ratio $M/L = 0.6$ (Bell & de Jong 2000) finally returns a $M_\star = 3.3 \times 10^{10} M_\odot$, which is above the average stellar mass of the hosts of nearby LGRBs (e.g., Kruhl et al. 2015; Perley et al. 2016; Schulze et al. 2015).

The spectrum of the nucleus of the host galaxy has been taken by the 6dF Galaxy Survey (Jones et al. 2004), which is a spectroscopic survey using the UK Schmidt telescope at Anglo-Australian Observatory.

The using of robotic positioning optical fibers allows the telescope to measure distances for more than 100,000 galaxies in 6 years. The rest-frame spectrum³ extracted from the final data release (DR3, Jones et al. 2009) is shown in Figure 6. It is noted that the spectrum shown in the figure is lack of absolute flux calibration. Nevertheless, the spectrum clearly shows that the host galaxy of GRB 171205A is a typical starforming galaxy with strong H α , H β , [N II] $\lambda\lambda 6548, 6583$, [S II] $\lambda\lambda 6727, 6731$, and weak [O III] $\lambda\lambda 4959, 5007$ emission lines. Figure 7 shows the occupation on the two empirical Baldwin-Phillips-Terlevich (BPT) diagrams for the host galaxy. The diagrams, which were originally proposed by Baldwin et al. (1981), and then refined by Veilleux & Osterbrock (1987), are traditionally used as a powerful tool to determine the dominant energy source in emission-line galaxies according to their emission-line ratios. By measuring the flux of each emission line through direct integration, the figure shows that the host galaxy is located within the locus of starforming sequence very well.

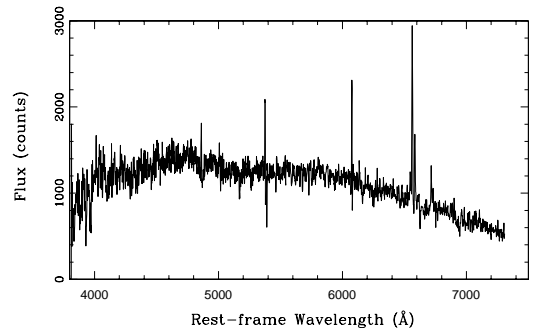


Figure 6. Rest-frame spectrum of the nucleus of the host galaxy of GRB 171205A/SN 2017iuk taken by the 6dF Galaxy Survey. Note that the spectrum is lack of absolute flux calibration.

We then estimate the star formation rate (SFR) from its near-ultraviolet detection. The brightness at the NUV band (peaked at $\sim 2800\text{\AA}$) of GALEX is reported to be $18.12 \pm 0.04\text{mag}$. At the be-

³ The rest-frame spectrum is transformed from the observed one by applying both Galactic extinction and Doppler corrections. See section 3.2.2 for the description in details.

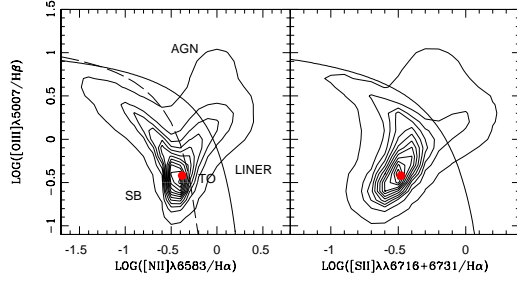


Figure 7. Two BPT diagnostic diagrams for the host galaxy of GRB 171205A/SN 2017iuk. The location of the burst is marked by the red circle in both panels, where the density contours are shown for a typical distribution of the narrow-line galaxies described in Heckman et al. (2004) and Kauffmann et al. (2003). Only the galaxies with $S/N > 20$ and the emission lines detected with at least 3σ significance are plotted. The solid lines in both panels mark the theoretical demarcation lines separating AGNs from star-forming galaxies proposed by Kewley et al. (2001). The long-dashed line in the left panel shows the empirical demarcation line proposed in Kauffmann et al. (2003), which is used to separate “pure” star-forming galaxies.

ginning, the NUV brightness is corrected for the Milkyway dust extinction from color excess through $A_{\text{NUV}} = R_{\text{NUV}}E(B - V)$. The parameter R_{NUV} is determined to be 6.62 (Fitzpatrick 1999), and updated to be 7.24 ± 0.08 by Yuan et al. (2013). The calibration of $\text{SFR} = 1 \times 10^{-28} L_{\text{NUV}} \text{ M}_{\odot} \text{ yr}^{-1}$, obtained by converting the relation from Kennicutt (1998) to the IMF in Kroupa (2001), is used to estimate SFR, where L_{NUV} is the NUV luminosity in unit of erg s^{-1} . With the extinction-corrected NUV brightness, we finally obtain a SFR of $\sim 1 \text{ M}_{\odot} \text{ yr}^{-1}$ for the host galaxy of GRB 171205A/SN 2017iuk, which is larger than the average value of the host galaxies of LGRBs at the similar redshift (e.g., Kruhl et al. 2015). With the estimated stellar mass of the host, the specific SFR (sSFR), defined as the SFR normalized to the total stellar mass, is inferred to be as low as $\sim 0.03 \text{ Gyr}^{-1}$. In fact, this value is at the lower end of the distribution of sSFR of samples of LGRB hosts (e.g. Savaglio et al. 2009; Japelj et al. 2016). Assuming a constant SFR over the growth history of the host, the growth timescale $t_{\star} = M_{\star}/\text{SFR}$ is estimated to be about 30 Gyr. This timescale is com-

parable to (or larger than) the Hubble time of the local universe, which implies a quiescent growth of the host galaxy of SN 2017iuk/GRB 171205A.

We finally estimate nuclear metallicity of the host galaxy of GRB 171205A/SN 2017iuk from the spectrum. The oxygen metallicity is simply calculated from the $N2$ method proposed in Pettini & Pagel (2004): $12 + \log(\text{O}/\text{H}) = 8.90 + 0.57N2$, where $N2 = \log([\text{NII}]/\text{H}\alpha)$, because the $[\text{N II}]/\text{H}\alpha$ line ratio is insensitive to both flux calibration and intrinsic dust extinction. The metallicity of the galaxy is inferred to be $12 + \log(\text{O}/\text{H}) = 8.69$, which equals to the solar gas phase value (Allende Prieto et al. 2001; Asplund et al. 2004). In fact, by using strong-line diagnostic, Kruhl et al. (2015) reported that the oxygen metallicities range from 7.0 to 9.0 for a sample of 44 LGRBs within a redshift range from 0.3 to 3.4.

In summary, GRB 171205A/SN 2017iuk occurred in an early type, high-mass, starforming galaxy with low sSFR and solar metallicity.

The authors thank the anonymous referee for a careful review and helpful suggestions that improved the manuscript. The study is supported by the National Basic Research Program of China (grant 2014CB845800) and by the Strategic Pioneer Program on Space Science, Chinese Academy of Sciences, Grant No.XDA15052600. JW is supported by the National Natural Science Foundation of China under grants 11473036 and 11773036. DX acknowledges the supports by the One-Hundred-Talent Program of the Chinese Academy of Sciences (CAS), by the Strategic Priority Research Program Multi-wavelength Gravitational Wave Universe of the CAS (No. XDB23000000), and by the National Natural Science Foundation of China under grant 11533003. Special thanks go to the staff at Xinglong Observatory as a part of National Astronomical Observatories, China Academy of Sciences for their instrumental and observational help, and to the allocated observers who allow us to finish the observations in ToO mode. This study is partially supported by the Open Project Program of the Key Laboratory of Optical Astronomy, NAOC, CAS. The study uses the data collected by 6dF Galaxy Survey which was carried out by the staff of the Australian Astronomical Observatory.

Facilities: Xinglong Observatory 2.16m telescope

Software: IRAF (Tody 1986, 1993), SYN++ (Thomas et al. 2011), SYNOW (Fisher 2000; Branch et al. 2000)

REFERENCES

- Allende Prieto, C., Barklem, P. S., Asplund, M., & Ruiz Cobo, B. 2001, *ApJ*, 558, 830
- Arnett, W. D. 1982, *ApJ*, 253, 785
- Arnett, W. D. 1996, *Supernovae and Nucleosynthesis: An Investigation of the History of Matter from the Big Bang to the Present*, Princeton University Press
- Asplund, M., Grevesse, N., Sauval, A. J., Allende Prieto, C., & Kiselman, D. 2004, *A&A*, 417, 751
- Baldwin, J. A., Phillips, M. M., & Terlevich, R. 1981, *PASP*, 93, 5
- Barthelmy, S. D., Cummings, J. R., D’Elia, V., et al. 2017, *GCN*, 22184, 1
- Bersten, M. C., Benvenuto, O. G., Orellana, M., & Nomoto, K. 2016, *ApJL*, 817, 8
- Bertin, E., & Arnouts, S. 1996, *A&AS*, 117, 393
- Bell, E. F., & de Jong, R. S. 2000, *MNRAS*, 312, 497
- Blondin, S., & Tonry, J. L. 2007, *ApJ*, 666, 1024
- Branch, D., Jeffery, D. J., Blaylock, M., & Hatano, K. 2000, *PASP*, 112, 217
- Bucciantini, N., Quataert, E., Arons, J., Metzger, B. D., & Thompson, T. A. 2007, *MNRAS*, 380, 1541
- Butler, N., Watson, A. M., Kutyrev, A., et al. 2017, *GCN*, 22182, 1
- Cano, Z. 2014, *ApJ*, 794, 121
- Cano, Z., Wang, S. Q., Dai, Z. G., & Wu, X. 2017, *AdAst*, 2017, 5
- Cano, Z., Johansson A. K. G., & Maeda, K. et al. 2016, *MNRAS*, 457, 2761
- Cardelli, J. A., Clayton, G. C., & Mathis, J. S. 1989, *ApJ*, 345, 245
- Choi, C., Im, M., Gak, L. S., & Pan-Starrs, et al. 2017, *GCN*, 22188, 1
- Cobb, B. E. 2017, *GCN*, 22270, 1
- Dai, Z. G., & Lu, T. 1998, *PhRvL*, 81, 4301
- Dai, Z. G., Wang, S. Q., Wang, J. S., Wang, L. J., & Yu, Y. W. 2016, *ApJ*, 817, 132
- D’Elia, V., Pian, E., Melandri, A., et al. 2015, *A&A*, 577, 116
- D’Elia, V., D’Ai, A., Lien, A. Y., & Sbarufatti, B. 2017, *GCN*, 22177, 1
- D’Elia, V., D’Ai, A., Melandri, A., et al. 2017, *GCN*, 22271, 1
- de Jong, R. S., Simard, L., Davies, R. L., et al. 2004, *MNRAS*, 355, 1155
- Della Valle, M., Chincarini, G., Panagia, N., et al. 2006, *Nature*, 444, 1050
- de Ugarte Postigo, A., Schulze, S., Bremer, M., et al. 2017a, *GCN*, 22187, 1
- de Ugarte Postigo, A., Izzo, L., Kann, D. A., Thoene, C. C., Pesev, P., Scarpa, R., & Perez, D. 2017b, *ATel*, 11038, 1
- Deng, J., Qiu, Y. L., & Hu, J. Y. 2001, *arXiv:astro-ph/0106404*
- Fan, Z., Wang, H. J., Jiang, X. J., et al., *PASP*, 128, 5005
- Filippenko, A. V. 1997, *ARA&A*, 35, 309
- Fisher, A. K. 2000, PhD thesis, Univ. Oklahoma
- Fitzpatrick E. L., 1999, *PASP*, 111, 63
- Frederiks, D., Golenetskii, S., Aptekar, R., et al. 2017, *GCN*, 22227, 1
- Fynbo, J. P. U., Watson, D., Thone, C. C., et al. 2006, *Nature*, 444, 1047
- Galama, T. J., Vreeswijk, P. M., van Paradijs, J., et al. 1998, *Nature*, 395, 670
- Gal-Yam, A., Fox, D. B., Price, P. A., et al. 2006, *Nature*, 444, 1053
- Greiner, J. Mazzali, P. A., Kann, D., et al. 2015, *Nature*, 523, 189
- Heckman, T. M., Kauffmann, G., Brinchmann, J., Charlot, S., Tremonti, C., & White, S. D. M. 2004, *ApJ*, 613, 109
- Hjorth, J., & Bloom, J. S. 2012, in *Gamma-Ray Bursts*, Vol. 51, ed. C. Kouveliotou, R. A. M. J. Wijers, & S. Woosley (Cambridge: Cambridge Univ. Press), 169
- Iwamoto, K., Nakamura, T., Nomoto, K., et al. 2000, *ApJ*, 534, 660
- Izzo, L., Selsing, J., Japelj, J., et al. 2017, *GCN*, 22180, 1
- Japelj, J., Vergani, S. D., Salvaterra, R. et al. 2016, *A&A*, 590, 129
- Jones, D. H., Read, M. A., Saunders, W., et al. 2009, *MNRAS*, 399, 683
- Jones, D. H., Saunders, W., Colless, M., et al. 2004, *MNRAS*, 355, 747
- Kasen, D., & Bildsten, L. 2010, *ApJ*, 717, 245
- Kauffmann, G., et al. 2003, *MNRAS*, 346, 1055
- Kennea, J. A., Sbarufatti, B., Burrows, D. N., et al. 2017, *GCN*, 22183, 1
- Kennicutt, R. C. Jr. 1998, *ARA&A*, 36, 189
- Kewley, L. J., Dopita, M. A., Sutherland, R. S., Heisler, C. A., & Trevena, J. 2001, *ApJ*, 556, 121
- Kroupa, P. 2001, *MNRAS*, 322, 231
- Kruhlér, T., Malesani, D., Fynbo, J. P. U., et al. 2015, *A&A*, 581, 125
- Laskar, T., Coppejans, D. L., Margutti, R., & Alexander, K. D. 2017, *GCN*, 22216, 1
- Lazzati, D., Covino, S., Ghisellini, G., et al. 2001, *A&A*, 378, 996
- MacFadyen, A. I., & Woosley, S. E. 1999, *ApJ*, 524, 262
- Maeda, K., Mazzali, P. A., Deng, J. S., et al. 2003, *ApJ*, 593, 931

- Mao, J., Ding, X., & Bai, J. -M. 2017a, GCN, 22186, 1
- Mao, J., Ding, X., & Bai, J. -M. 2017b, GCN, 22195, 1
- Masetti, N., Palazzi, E., Pian, E., et al. 2005, A&A, 438, 841
- Massey, P., Strobel, K., Barnes, J. V., et al. 1988, ApJ, 328, 315
- Mazzali, P. A., Deng, J., Nomoto, K., et al. 2006, Nature, 442, 1018
- Mazzali, P. A., McFadyen, A. I., Woosley, S. E., Pian, E., & Tanaka, M. 2014, MNRAS, 443, 67
- Melandri, A., D’Avanzo, P., di Fabrizio, L., Padilla, C., & D’Elia, V. 2017, GCN, 22189, 1
- Metzger, B. D., Margalit, B., Kasen, D., & Quataert, E. 2015, MNRAS, 454, 3311
- Nakamura, T., Mazzali, P. A., Nomoto, K., & Iwamoto, K. 2001, ApJ, 550, 991
- Perley, D. A., Schulze, S., & de Ugarte Postigo, A. 2017, GCN, 22252, 1
- Perley, D. A., Tanvir, N. R., Hjorth, J., et al. 2016, ApJ, 817, 8
- Pian, E., Mazzali, P. A., Masetti, N., et al. 2006, Nature, 442, 1011
- Prentice, S., Mazzali, P., Smartt, S. J. et al. 2017, ATel, 11060, 1
- Sahu, D. K., Anupama, G. C., Chakradhari, N. K., Srivastav, S., Tanaka, M., Maeda, K., & Nomoto, K. 2018, MNRAS, 475, 2591
- Savaglio, S., Glazebrook, K., & Le Borgne, D. 2009, ApJ, 691, 182
- Schlaflly, E. F., & Finkbeiner, D. P. 2011, ApJ, 737, 103
- Schulze, S., Chapman, R., Hjorth, J., et al. 2015, ApJ, 808, 73
- Smith, I. A., & Tanvir, N. R. 2017, GCN, 22242, 1
- Sukhbold, T., Ertl, T., Woosley, S. E., Brown, J. M., & Janka, H.-T. 2016, ApJ, 821, 38
- Thomas, R. C., Nugent, P. E., & Meza, J. C. 2011, PASP, 123, 237
- Tody, D. 1986, Proc. SPIE, 627, 733
- Tody, D. 1993, in ASP Conf. Ser. 52, adass II, ed. R. J. Hanisch, R. J. V. Brissenden, & J. Barnes (San Francisco, CA: ASP), 173
- Veilleux, S., & Osterbrock, D. E. 1987, ApJS, 63, 295
- Wang, L. J., Yu, H., Liu, L. D., et al. 2017, ApJ, 837, 128
- Wang, J., Xin, L. P., Qiu, Y. L., Xu, D. W., & Wei, J. Y. 2018, ApJ, 855, 91
- Wang, S. Q., Wang, L. J., Dai, Z. G., & Wu, X. F. 2015, ApJ, 799, 107
- Woosley, S. E. 1993, ApJ, 405, 273
- Woosley, S. E., & Bloom, J. S. 2006, ARA&A, 44, 507
- Woosley, S. E., & Heger, A. 2006, ApJ, 637, 914
- Yuan, H. B., Liu, X. W., & Xiang, M. S. 2013, MNRAS, 430, 2188
- Zhang, B., & Dai, Z. G. 2010, ApJ, 718, 841